New Pretreatment Methods for Visible–Near-Infrared Calibration Modeling of Air-Dry Density of *Ulmus pumila* Wood

Ying Li Brian K. Via Qingzheng Cheng
Jinghan Zhao Yaoxiang Li

Abstract

Due to the multidimensional complexity and redundancy between wavelengths in the visible and near infrared (Vis-NIR) region, the speed and accuracy of data analysis can be affected. This study aims to investigate the feasibility of simplifying high dimensional data based on transformation of the spectra and local correlation maximization (LCM). These two methods will be applied to determine the prediction accuracy of air-dry density of *Ulmus pumila* wood. In this study, the reflectance spectra (Refl.) were subjected to the reciprocal (1/Refl.) and logarithm reflectance to improve the spectra signal for prediction. LCM was developed for selecting spectral sensitive regions that were important in the prediction of density. A local correlation coefficient (r) criterion was developed such that if the $r \geq 0.75$ (between wavelength and density), then partial least squares and support vector machine (SVM) were employed as the prediction method. Likewise, 2D correlation spectroscopy plots were used to further reduce the data matrix by removing redundant wavelengths. The results showed that (1) although the sensitive region of density was different, the region of $r \geq 0.80$ was mainly in the Vis and NIR spectral region. Additionally, the performance of models developed from the sensitive region was better than that of data used from the less-sensitive region. (2) The SVM model was optimized by a genetic algorithm based on the log (1/Refl.) of the sensitive region. In conclusion, it was found that the spectral transformation presented better density estimation results ($R_c^2 = 0.909$, root mean square error of calibration = 0.014) than when less sensitive wavelengths were used in the data matrix.

Wood density is a critical indicator of wood quality and variation in density can have a profound effect on end use applications (Prasetyo et al. 2018). Additionally, tissue density correlates with the morphological, physiological, and mechanical properties of wood as a result of strong intercorrelations with microfibril angle, stiffness, and strength (Wu et al. 2009, Li and Jiang 2013, Dahlen et al. 2018). The tree can begin to produce tissue of variable density as early as 3 months old, while genetics can be used to fine-tune tree density for improved product performance (Gonçalves et al. 2019). Although the traditional determination of density through gravimetric means has the best accuracy, it has been shown that visible and near infrared (Vis-NIR) spectroscopy can provide good in situ estimation of within-ring density without having to destroy the sample for conventional testing (Giroud et al. 2015).

Vis-NIR can also reduce the cost and time of traditional density-measurement methods. Vis-NIR spectroscopy—a simple, fast, and nondestructive method—has been widely applied to agriculture, petrochemical industries, food safety, and life sciences (Verbeek et al. 2014, Li et al. 2017, Siriphollakul et al. 2017, Zhuang et al. 2017). Many studies have demonstrated that Vis-NIR technology can be used for the analysis of components, species and habitat identification, and detection of wood preservation or modification in the field of forestry (Yang et al. 2012; Dou et al. 2016; Li et al. 2016, 2018a; Kurata 2017). The qualitative and quantitative relationship between spectra and wood properties can be obtained using chemometric methods. However, the speed and accuracy of spectral data analysis can be

The authors are, respectively, Graduate Researcher, College of Engineering and Technol., Northeast Forestry Univ., Harbin, China (yingli@nefu.edu.cn); Director and Research Fellow, Forest Products Development Center, SFWS, Auburn Univ., Auburn, Alabama (brianvia@auburn.edu, qzc0007@auburn.edu); and Graduate Researcher and Professor, College of Engineering and Technol., Northeast Forestry Univ., Harbin, China (1874670424@qq.com, yaoxiangli@nefu.edu.cn [corresponding author]). This paper was received for publication in January 2019. Article no. 19-00004.
©Forest Products Society 2019.
Forest Prod. J. 69(3):188–194.
doi:10.13073/FPJ-D-19-00004

http://prime-pdf-watermark.prime-prod.pubfactory.com/ | 2024-12-26

complex and slow because of the multidimensional nature and redundancy of the spectral data. Reduction in the spectra to only those wavelengths necessary for prediction could be useful in speeding up the process; however, a reduction in the data matrix content could result in lower prediction accuracy, and ways to maintain predictability with less spectral information are a key challenge when using Vis-NIR spectroscopy.

In the field of agriculture, Sun and Cheng (2010) found that leaf chlorophyll was highly correlated with their second derivation spectra at wavelengths 700, 670, 600, 500, 490, 440, and 410 nm. Guo et al. (2015) predicted paddy soil available nitrogen (AN) content using sensitive wavelengths (694, 2,058, and 2,189 nm) through 16 kinds of mathematical transformations and obtained good results (best $R = 0.748$). It can be found that the spectral sensitive region of a particular trait can be used for calibration and simplifying spectral data can result in good prediction accuracy in the agricultural sector. However, to our knowledge, we could not find other studies that used these transformation techniques to predict wood density, and feel this research would be useful to industry and academic entities.

In this study, *Ulmus pumila* wood samples were used for spectra collection and air-dry density determination. Different spectral transformations were first applied to the wood spectra to improve the sensitivity of the prediction model. Local correlation maximization (LCM) methods (Zhang et al. 2017) were developed for selecting the spectral sensitive region most correlated to air-dry density. The chosen sensitive region was used for model establishment with linear (partial least squares, PLS) and nonlinear methods (support vector machine, SVM), respectively.

Materials and Methods

Sample preparation

Ulmus pumila L. is one of the major commercial tree species in northeastern China (Xu et al. 2000). Eight *Ulmus pumila* trees were harvested from the location 126°30′–127°16′E, 42°06′–42°48′N, Jilin Province, China. Five-centimeter disks were cut from each tree at 1-m intervals along the stem with 69 total discs prepared for model calibration and spectra collection. The disks were air-dried in an environment controlled laboratory (temperature: 20°C ± 2°C; relative humidity: 65% ± 3%). Additionally, to reduce the roughness of sample surface, the cross-sections of all disks were polished using an electric plane.

Vis-NIR spectra collection and air-dry density measurement

Cell spacing, anatomy position–frequency, and annual ring width influence wood density, and these variables are more obvious when viewed in the cross-section. Therefore, the Vis-NIR spectra were collected from a cross-section of each sample using a LabSpec Pro FR/A114260 (Analytical Spectral Devices, Inc., Boulder, Colorado). Additionally, a traditional fiber-optic probe was replaced with a glare probe to obtain more spectral information. Before spectra collection, the spectrometer was calibrated with a commercial white plate made of polytetrafluoroethylene. Each sample was scanned three times and the average spectrum was regarded as the original spectrum. The air-dry density of the samples were measured at 12 percent moisture content (Standardization Administration of China 2009).

Spectral data analysis

Spectra of transformations.—Even though the whole process of spectra collection was determined in a controlled environment, there can still be uncontrollable sources of error during spectra collection such as spectrometer signal, and environmental influence on data quality and corresponding accuracy and precision (Via et al. 2005). Therefore, the reflectance spectra (Refl.) were subjected to reciprocal (1/Refl.) and logarithm reflectance (log(Refl.) and log(1/Refl.)) to eliminate multiplicative effects (He et al. 2006). The spectra of transformations were implemented by using Matlab R2014b (MathWorks, Natick, Massachusetts).

Selection of sensitive regions to air-dry density variation.—To simplify the complexity of modeling for multidimensional spectral data, the reflectance spectra (Refl.) was subjected to reciprocal and logarithm transformations. The LCM was used for selection of important wavelengths in the prediction of air-dry density. The region was deemed statistically important if the local correlation coefficient (r) was greater than or equal to 0.75 ($r \geq 0.75$) when a correlation matrix was run between the spectra and density. The LCM was also implemented in Matlab R2014b (MathWorks).

In this study, 69 samples were randomly divided into a calibration set (50 samples) and a prediction set (19 samples). Given that $X(m,n)$ is the matrix of the Vis-NIR spectral data, x_{ij} is the vector of $X(m,n)$, and y_i is the air-dry density value, where m is the number of samples ($m = 50$ for calibration set) and n is the wavelength of Vis-NIR spectra ($n = 2{,}151$). The LCM was used to analyze the correlation between x_{ij} and y_i, and local correlation coefficients (r) for different spectra of transformations were obtained. High correlation should consist of high r (Mo 2015). The computation equations of r is shown as follows:

$$r_j = \sum_{i=1}^{m}(x_{ij} - \overline{x_j})(y_i - \overline{y}) \Big/ \sqrt{\sum_{i=1}^{m}(x_{ij} - \overline{x_j})^2 \sum_{i=1}^{m}(y_i - \overline{y})^2} \quad (1)$$

where $\bar{x_j}$ and $\bar{y}$ represent the mean of the vector of the Vis-NIR spectral data and the air-dry density value, respectively, which are given by

$$\overline{x_j} = \sum_{i=1}^{m} x_{ij}/m \quad (2)$$

$$\overline{y} = \sum_{i=1}^{m} y_i/m \quad (3)$$

where $i = 1, 2 \ldots m$, $j = 1, 2 \ldots n$, the meanings of m and n are the same with Eq. (1).

Vis-NIR model calibration and evaluation.—Vis-NIR technology is an indirect nondestructive method in which the method for the prediction of sample properties can be obtained through advanced chemometric procedures. In this study, the performance of linear and nonlinear methods, including PLS regression and SVM, were compared. PLS is a useful linear method in the modeling of multidimension spectral data. It simplifies spectral data and selects variables by correlating the independent variable y_i with the Vis-NIR model. PLS was implemented in The Unscrambler V10.4 (CAMO Software AS, Oslo, Norway). PLS does inflate the

http://prime-pdf-watermark.prime-prod.pubfactory.com/ | 2024-12-26

error of the peaks in the loading vector; however, transformations such as those being explored have been shown to minimize this error (Via et al. 2014).

The SVM was first proposed to solve classification problems. In recent years, it has been shown that SVM is a powerful method for classification and regression in agriculture, life sciences, and other fields (Hajikhodaverdikhan et al. 2018, Oguntunde et al. 2018, Zhi et al. 2018). SVM was used for Vis-NIR model calibration because of the advantages of processing small sample sets and high dimensional spaces effectively. Grid search (GS) and a genetic algorithm (GA) were employed to optimize the cost parameter c and the radial basis function (RBF) kernel parameter gamma. The SVM was implemented in Matlab R2014b (MathWorks). It is hypothesized that SVM may be superior to more traditional methods of transformation that is commonly used during classification (Kurata 2017) and is the subject of this research.

After the sensitive regions that correlated to air-dry density were selected using the LCM algorithm, the PLS and SVM transformations were executed to establish Vis-NIR models, respectively. Additionally, the performance of the band with higher local correlation coefficients ($r \geq 0.80$) in sensitive and less-sensitive regions ($0.7 < r < 0.75$) were compared. The performance of calibration and prediction models was evaluated based on determination coefficients (R^2), root mean square error (RMSE), standard error of estimation (SEE), mean absolute percentage error (MAPE), and residual predictive deviation (RPD). Lower RMSE, SEE, MAPE and higher R^2, RPD values indicate higher model accuracy (Yan et al. 2013). The criteria were calculated according to Eqs. (4) to Eq. (8), respectively.

$$R^2 = 1 - \sum_{i=1}^{m}(y_i - \hat{y}_i)^2 / \sum_{i=1}^{m}(y_i - \bar{y})^2 \quad (4)$$

$$\mathrm{RMSE} = \sqrt{\sum_{i=1}^{m}(y_i - \hat{y}_i)^2 / m} \quad (5)$$

$$\mathrm{SEE} = \sqrt{\sum_{i=1}^{m}\left(y_i - \hat{y}_i - \frac{1}{m}\sum_{i=1}^{m}(y_i - \hat{y}_i)\right)^2 / m - 1} \quad (6)$$

$$\mathrm{MAPE} = \sum_{i=1}^{m} |(y_i - \hat{y}_i)/y_i| / m \times 100\% \quad (7)$$

$$\mathrm{RPD} = SD/SEE \quad (8)$$

where SD is standard deviation of prediction set.

Results and Discussion

Statistical characteristics of wood air-dry density

The statistical characteristics of the samples are illustrated in Table 1. The air-dry density ranged from 0.909 to 1.128 g/cm^3, with an average value of 1.062 g/cm^3. The standard deviation (SD) in the calibration and prediction set were similar and smaller than 0.05. Additionally, there was low negative skewness and positive kurtosis, indicating low scatter distribution.

Correlations between wavelength variables

As shown in Figures 1A through 1D, regardless of various spectral transformations, a relatively high correlation was obtained within each of the two regions (i.e., near 500 to 1875 nm, and 1800 to 2500 nm). It can be seen that the Vis-NIR spectral region showed high redundancy and selecting only highly sensitive variables related to the properties of interest is needed for simplifying the high-dimensional spectral-data matrix.

Sensitive region of air-dry density analysis

There was high redundancy of wavelength variables (Fig. 1), so the LCM was performed for selecting only those sensitive regions of air-dry density based on local correlation coefficients between different spectra and air-dry density. The correlation coefficients and frequency statistics are shown in Figure 2 and Table 2, respectively.

It was observed that the correlation levels between wavelengths were dependent on the type of spectra transformation performed. This suggests there is the potential for different transformation methods to yield better calibration models. In terms of reflectance spectra (Refl.), there was a negative relationship between Refl. spectra and air-dry density in the wavelength range of 593 to 813 and 1,148 to 1,036 nm, while the other bands exhibited a positive correlation.

For the 1/Refl. spectral data, there were negative correlations in the Vis-NIR spectral region (350 to 2,500 nm). Compared with the Refl. spectral data, the local correlation coefficients in the NIR spectral region of 1,897 to 2,476 nm were significant—they showed values up to 0.70.

Compared with Refl. spectral data, the log(Refl.) spectra improved the correlation in the Vis spectral region of 350 to 401 nm; among which, the correlation coefficient located in 367 nm was increased from 0.72 to 0.78, and the others were all improved to >0.80. Additionally, the correlations in the wavelength range of 1,890 to 2,438 nm were improved. Comparing 1/Refl. spectral data, it could be found that the r located in 1,922 nm, 1,932 nm, and 1,933 nm were improved to >0.80. According to the properties of logarithmic function, the distributions of r for log(1/Refl.) and log(Refl.) spectral data were symmetrical to wavelength axis.

Figure 3 shows the distribution of the sensitive wavelengths of air-dry density ($r \geq 0.75$). Although the sensitive regions were different for Refl., 1/Refl., log(Refl.), and log(1/Refl.) spectral data, the distribution of $r \geq 0.80$ were located at the Vis spectral region of 350 to 391 nm and NIR spectral region of 1,932 to 1,933 nm. The Vis spectral range was assigned to polycyclic aromatic hydrocarbons and their derivatives (Workman and Weyer 2007). As for the NIR spectral region, there was a narrow band associated with density variance. However, this band was quite close to the absorption peak of lignin and cellulose as associated with 1,900 nm (Üner et al. 2011). Additionally, it is associated with the combination of O–H deformation and stretching vibration (Schwanninger et al. 2011, Wójciak et al. 2014).

Establishment of Vis-NIR calibration models

To better analyze the effect of important spectral regions on the prediction of air-dry density, linear (PLS) and

http://prime-pdf-watermark.prime-prod.pubfactory.com/ | 2024-12-26

Table 1.—Air-dry density statistics of Ulmus pumila *wood.*

Sample set	No. of samples	Max. (g/cm^3)	Min. (g/cm^3)	Avg. (SD) (g/cm^3)	Skewness	Kurtosis
Calibration set	50	1.128	0.909	1.061 (0.047)	−1.461	2.743
Prediction set	19	1.120	0.962	1.065 (0.039)	−1.079	1.593
Total	69	1.128	0.909	1.062 (0.045)	−1.408	2.644

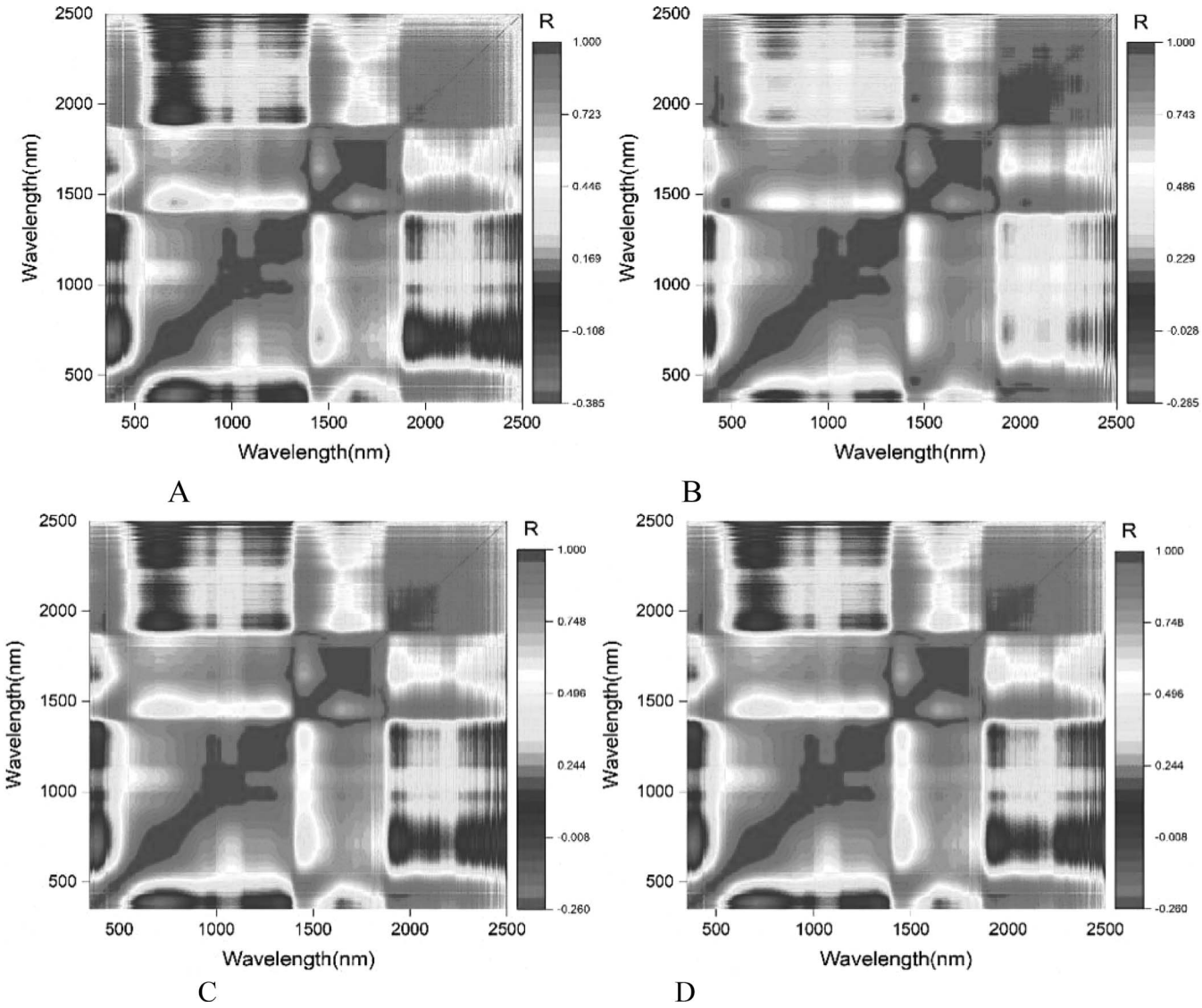

Figure 1.—2D correlation coefficient plot between different spectra of transformations and corresponding wavelength variables. (A) Refl. spectral data; (B) 1/Refl. spectral data; (C) log(Refl.) spectral data; (D) log(1/Refl.) spectral data.

nonlinear (SVM) methods were employed. The results of the PLS model are shown in Table 3.

Regardless of the transformation, the performance of the model that uses the sensitive region ($r \geq 0.75$) to predict air-dry density was better than when the less-sensitive region was included (Table 3). Compared with the less-sensitive region, the accuracy of models developed from very sensitive regions was indeed better. However, as for 1/Refl. spectral data, the accuracy of models developed from less-sensitive regions ($R_c^2 = 0.677$) was comparable to the highly correlated region in the sensitive region ($R_c^2 = 0.675$; Table 3). This may be due to the fact that the number of variables selected into models of $0.70 < r < 0.75$ (no. = 347) were larger than others.

For the linear models, the best performance was from the log(1/Refl.) spectral data transformation on the sensitive region, with R_c^2 and root mean square error of calibration values of 0.870 and 0.017, respectively (Table 3). The next best model was when the log(Refl.) spectra transformation was used. Compared with the models using the less-sensitive region, for the models that used the highly correlated region, the R_c^2 was increased by 33.03 and 11.54 percent, respectively (Table 3). This demonstrated that the log(1/Refl.) spectral transformation coupled with the

http://prime-pdf-watermark.prime-prod.pubfactory.com/ | 2024-12-26

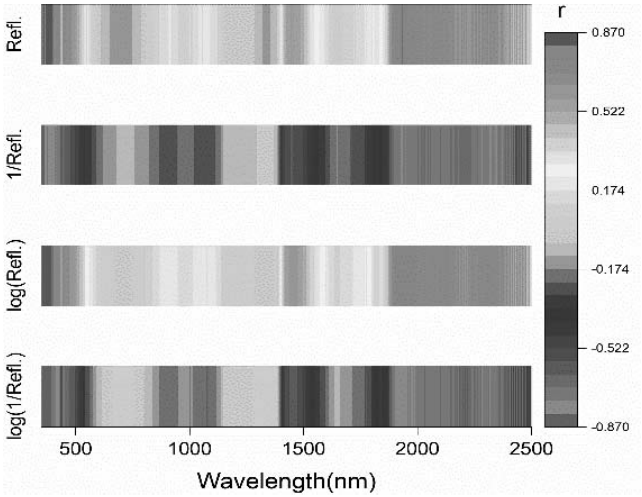

Figure 2.—2D local correlation coefficient plot between different spectra of transformations and air-dry density.

Table 2.—Local correlation coefficients statistics for different spectral transformations.

Spectra of transformations	$r > 0.70$ (no.)	$r > 0.75$ (no.)	$r > 0.80$ (no.)	Max. r (nm)
Refl.	294	131	46	375
1/Refl.	473	126	32	354
log(Refl.)	453	192	54	355
log(1/Refl.)	453	192	54	355

sensitive region of air-dry density not only reduced the dimension of the spectral data matrix, but also the model obtained a good fit. This was an indication that the quality of the information was perhaps improved while the amount of information needed for collection or analysis was reduced.

The improved models developed from spectra only from the sensitive region performed well, so this same reduced data matrix was used to build nonlinear models using SVM. The GS and GA were used for the optimization of the cost parameter c and RBF kernel parameter gamma. The results of SVM models were shown in Table 4.

For the different methods of transformation, performance of the SVM models optimized by GA was superior to that of the GS-optimized SVM and PLS models; R_c^2 were all >0.75 (Table 4). Although the SVM is a nonlinear modeling method, the results of SVM optimized by GS were inferior to the PLS models, except for log(1/Refl.) spectra. This could be caused by the nonheuristic algorithm of GS, which searches the cost parameter c and RBF kernel parameter gamma in a limited region. It should be noted that the reasonable selection of parameters is critical in modeling. Among the SVM models, the combination of log(1/Refl.) spectra and GA method achieved the best performance; the cost parameter c and RBF kernel parameter gamma were 99.653 and 0.001, respectively (Fig. 4). In comparison with GS-optimized SVM model and PLS model, the R_c^2 was increased by 0.44 and 4.48 percent, respectively.

The relationship between measured air-dry values and predicted values based on GA-optimized SVM models using log(1/Refl.) spectra are shown in Figure 5. The SVM model

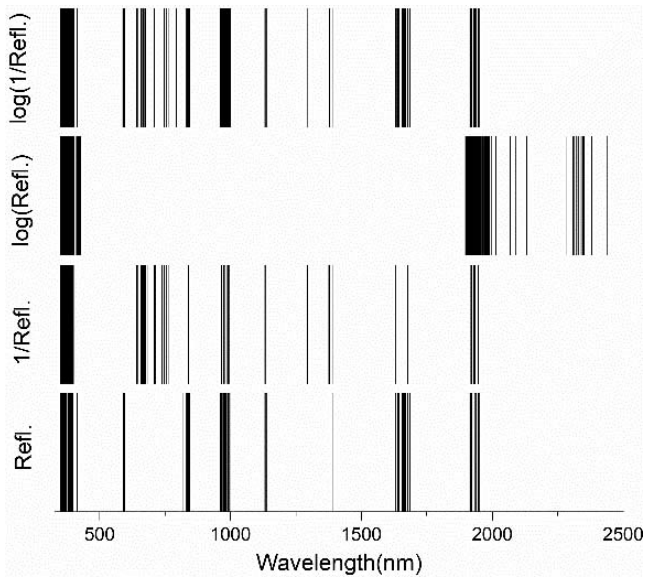

Figure 3.—Sensitive region of air-dry density for different spectra of transformations.

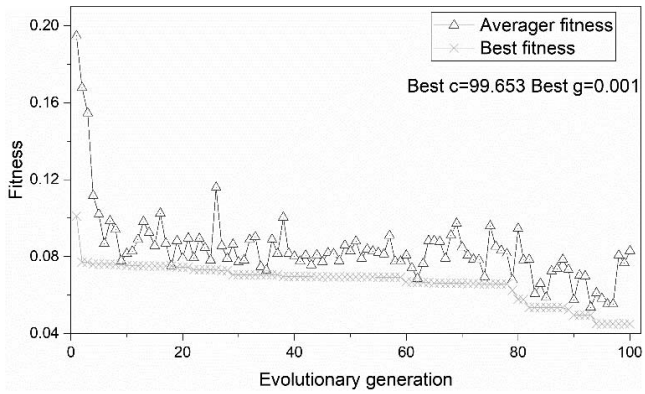

Figure 4.—The iterative fitness trend of the genetic algorithm–optimized support vector machine for searching the optimization parameter.

optimized by GA obtained good predictive performance, laying the basis for air-dry density estimation.

After a review of the current literature, few studies have focused on the comparison of different transformations of spectra prior to modeling wood properties, the most common spectra data matrix being the reflectance spectra or log(1/R) spectra (Ramirez et al. 2015, Inagaki et al. 2018, Li et al. 2018b). In the field of agriculture, Sun et al. (2018) applied five spectral transformations including reflectance spectra, reciprocal, reciprocal logarithm, first-order, and second-order differential spectra to predict the soil organic carbon (SOC) of samples from a coal mining area. They found that the spectral reflectance obtained the best results when predicting SOC, which differed from the results of this study, suggesting that there is not a universal transformation that works for all scenarios. This difference may be due to the difference of properties between soil and wood. In addition, the different denoising methods, such as Savitaky–Golay (SG), multiple scattering correction (MSC), and the

http://prime-pdf-watermark.prime-prod.pubfactory.com/ | 2024-12-26

Table 3.—Statistics results of partial least squares for spectra of transformations.

Spectra of transformations	Less-sensitive region ($0.70 < r < 0.75$)				Sensitive region ($r \geq 0.75$)				A highly correlated region in sensitive region ($r \geq 0.80$)			
	No.	R_c^2	RMSEC[a]	SEC[b]	No.	R_c^2	RMSEC[a]	SEC[b]	No.	R_c^2	RMSEC[a]	SEC[b]
Refl.	163	0.682	0.027	0.027	131	0.778	0.022	0.022	46	0.754	0.023	0.024
1/Refl.	347	0.677	0.027	0.027	126	0.781	0.022	0.022	32	0.675	0.027	0.027
log(Refl.)	261	0.576	0.031	0.031	192	0.824	0.020	0.020	54	0.781	0.022	0.022
log(1/Refl.)	261	0.654	0.028	0.028	192	0.870	0.017	0.017	54	0.780	0.022	0.022

[a] RMSEC = root mean square error of calibration.
[b] SEC = standard error of calibration.

Table 4.—Statistics results of support vector machine for sensitive region (r $\geq$ 0.75).

Spectra of transformations	Grid search			Genetic algorithm		
	R_c^2	RMSEC[a]	SEC[b]	R_c^2	RMSEC[a]	SEC[b]
Refl.	0.769	0.023	0.023	0.840	0.019	0.019
1/Refl.	0.671	0.027	0.027	0.765	0.023	0.023
log(Refl.)	0.763	0.023	0.023	0.827	0.020	0.020
log(1/Refl.)	0.905	0.014	0.015	0.909	0.014	0.014

[a] RMSEC = root mean square error of calibration.
[b] SEC = standard error of calibration.

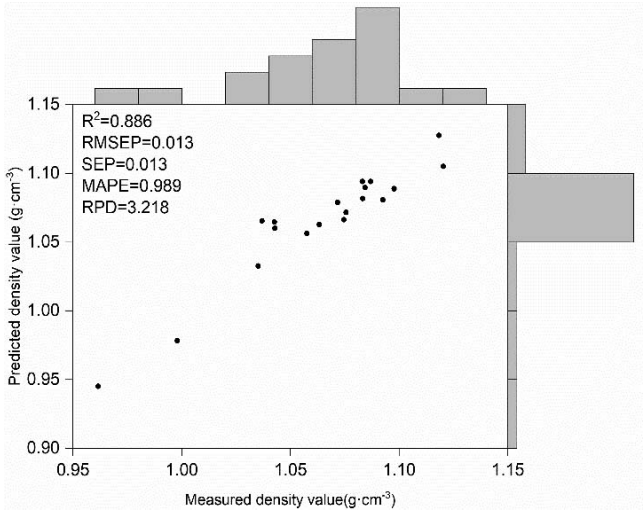

Figure 5.—The results of genetic algorithm-optimized support vector machine model for sensitive region (r $\geq$ 0.75). RMSEP is root mean square error of prediction; SEP is standard error of prediction; MAPE is mean absolute percentage error; RPD is residual predictive deviation.

combination of SG and MSC, were performed before the spectra of transformation in their study.

Vis-NIR spectral data often contain redundant information that makes modeling more difficult. To assist with this problem, the LCM was used to analyze which wavelength regions were sensitive to variation in air-dry density. It could be observed that the performance of models developed from the sensitive region was better than that of the less-sensitive region, regardless of the different spectral transformations. This is because specific absorption bands can be assigned to various wood chemical constituents such as lignin, cellulose, and hemicellulose (Cheng et al. 2018); and the spectra sensitive regions simply covary with this underlying chemistry. Additionally, the prediction accuracy of SVM model optimized by GA was >0.85 and superior to the results of Schimleck et al. (2018), which demonstrated the feasibility of simplifying the multidimension spectral data and keeping a good-fitting model based on LCM and GA-optimized SVM model.

Conclusions

This study investigated the effects of various combinations of spectral transformations and LCM algorithms on wood air-dry density estimation based on Vis-NIR spectroscopy. The correlation between density and spectra varied with the method of spectra transformation. The LCM algorithm selected the most statistically sensitive region of the spectra in relation to air-dry density ($r \geq 0.75$) for Refl., 1/Refl., log(Refl.), and log(1/Refl.). Although the sensitive regions were different, there existed the same band (i.e., the region of $r \geq 0.80$) in Vis spectral region (i.e., 350 to 391 nm) and NIR spectral region (i.e., 1,932 to 1,933 nm), which was critical for the prediction of density. The linear (PLS) and nonlinear (SVM) modeling results using sensitive regions demonstrated better accuracy than less-sensitive regions in density estimation, regardless of spectral transformations. In comparison with PLS and SVM models, the performance of GA-optimized SVM model based on the sensitive region was better than PLS and the GS-optimized SVM model. In conclusion, this study improved the prediction and accuracy of the air-dry density models by selecting only those wavelengths that were most sensitive.

Acknowledgments

This research was supported by the Fundamental Research Funds for Central Universities (Grant number 2572017AB04) and the National Key R&D Program of China (Grant number 2017YFC0504103).

Literature Cited

Cheng, Q., C. Zhou, W. Jiang, X. Zhao, B. K. Via, and H. Wan. 2018. Mechanical and physical properties of oriented strand board exposed to high temperature and relative humidity and coupled with near-infrared reflectance modeling. *Forest Prod. J.* 68(1):78–85.

Dahlen, J., F. Antony, L. R. Schimleck, and R. F. Daniels. 2018. Relationships between static mechanical properties and SilviScan measured wood properties in loblolly pine. *Forest Prod. J.* 68(1):37–42.

Dou, G., G. S. Chen, and P. Zhao. 2016. Research and implementation of wood species recognition system with wood near infrared spectral reflection features. *Spectrosc. Spect. Anal.* 36(8):2425–2429.

Giroud, G., M. Defo, J. Bégin, and C. H. Ung. 2015. Application of near-infrared spectroscopy to determine the juvenile–mature wood transition in black spruce. *Forest Prod. J.* 65(3):129–138.

http://prime-pdf-watermark.prime-prod.pubfactory.com/ | 2024-12-26

Gonçalves, R., R. G. M. Lorensani, M. Ruy, N. S. Veiga, G. Müller, C. da Silva Alves, and G. A. Martins. 2019. Evolution of acoustical, geometrical, physical, and mechanical parameters from seedling to cutting age in Eucalyptus clones used in the pulp and paper industries in Brazil. *Forest Prod. J*. 69(1):5–16.

Guo, X., Y. C. Ye, B. Y. Xie, L. H. Kuang, and W. Xie. 2015. Inversion of available nitrogen content in hilly paddy soil of southern China based on hyperspectral characteristics. *Remote Sens. Land Resour*. 27(2):94–99.

Hajikhodaverdikhan, P., M. Nazari, M. Mohsenizadeh, S. Shamshirband, and K. W. Chau. 2018. Earthquake prediction with meteorological data by particle filter-based support vector regression. *Eng. Appl. Comp. Fluid*. 12(1):679–688.

He, T., J. Wang, Z. J. Lin, and Y. Cheng. 2006. Spectral features of soil organic matter. *Geomat*. *Info Sci. Wuhan Univ*. 31(11):975–979.

Inagaki, T., H. Yonenobu, Y. Asanuma, and S. Tsuchikawa. 2018. Determination of physical and chemical properties and degradation of archeological Japanese cypress wood from the Tohyamago area using near-infrared spectroscopy. *J. Wood Sci*. 64(4):347–355.

Kurata, Y. 2017. Nondestructive classification analysis of wood soaked in seawater by using near-infrared spectroscopy. *Forest Prod. J*. 67(1):63–68.

Li, J. Y., X. L. Chu, P. Chen, and S. B. Tian. 2017. Application of spectral automatic retrieval algorithm on the rapid establishment of gasoline spectral database. *Acta Petrol. Sin. (Petroleum Processing Section)* 33(1):131–137.

Li, Y., Y. X. Li, W. B. Li, and L. C. Jiang. 2018a. Model optimization of wood property and quality tracing based on wavelet transform and NIR spectroscopy. *Spectrosc. Spect*. *Anal*. 38(5):1384–1392.

Li, Y., Y. X. Li, H. K. Xu, and L. C. Jiang. 2016. Model calibrating for NIRS-based oak wood air-dry density prediction with denoising pretreatment. *J. Nanjing Forestry Univ*. 40(6):148–156.

Li, Y., B. Via, Q. Z. Cheng, and Y. X. Li. 2018b. Lifting wavelet transform de-noising for model optimization of Vis-NIR spectroscopy to predict wood tracheid length in trees. *Sensors-Basel*. 18:4306.

Li, Y. X. and L. C. Jiang. 2013. Modeling wood density with two-level linear mixed effects models for Dahurian larch. *Sci. Silvae Sinicae* 49(7):91–98.

Mo, Z. L. 2015. Prediction model for infectious disease incidence based on wavelet neural network optimized by genetic algorithm. Master's thesis. Chong Qing Medical University, Chong Qing, China. 66 pp.

Oguntunde, P. G., G. Lischeid, and O. Dietrich. 2018. Relationship between rice yield and climate variables in southwest Nigeria using multiple linear regression and support vector machine analysis. *Int. J. Biometeorol*. 62(3):459–469.

Prasetyo, A., H. Aiso, F. Ishiguri, I. Wahyudi, I. P. G. Wijaya, J. Ohshima, and S. Yokota. 2018. Growth characteristics and wood properties of two interspecific Eucalyptus hybrids developed in Indonesia. *Forest Prod. J*. 68(4):436–444.

Ramirez, J. A., J. M. Posada, I. T. Handa, G. Hoch, M. Vohland, C. Messier, and B. Reu. 2015. Near-infrared spectroscopy (NIRS) predicts non-structural carbohydrate concentrations in different tissue types of a broad range of tree species. *Methods Ecol. Evol*. 6(9):1018–1025.

Schimleck, L., F. Antony, C. Mora, and J. Dahlen. 2018. Comparison of whole-tree wood property maps for 13- and 22-year-old Loblolly Pine. *Forests* 9(6):287.

Schwanninger, M., J. C. Rodrigues, and K. Fackler. 2011. A review of band assignments in near infrared spectra of wood and wood components. *J. Near Infrared Spec*. 19(5):287–308.

Siriphollakul, P., K. Nakano, S. Kanlayanarat, S. Ohashi, R. Sakai, R. Rittiron, and P. Maniwara. 2017. Eating quality evaluation of Khao Dawk Mali 105 using near-infrared spectroscopy. *LWT-Food Sci. Technol*. 79:70–77.

Standardization Administration of China (SAC). 2009. Method for determination of the density of wood. GB/T 1933-2009. SAC, Beijing.

Sun, L. and L. J. Cheng. 2010. Analysis of spectral response of vegetation leaf biochemical component. *Spectrosc. Spect*. *Anal*. 30(11):3031–3035.

Sun, W. J., X. J. Li, and B. B. Niu. 2018. Prediction of soil organic carbon in a coal mining area by Vis-NIR spectroscopy. *PLOS One* 13(4):e0196198.

Üner, B., İ. Karaman, H. Tanrıverdi, and D. Özdemir. 2011. Determination of lignin and extractive content of Turkish Pine (Pinus brutia Ten.) trees using near infrared spectroscopy and multivariate calibration. *Wood Sci. Technol*. 45(1):121–134.

Verbeek, F. P., S. L. Troyan, J. S. Mieog, G. J. Liefers, L. A. Moffitt, M. Rosenberg, J. Hirshfield-Bartek, S. Gioux, C. J. van de Velde, A. L. Vahrmeijer, and J. V. Frangioni. 2014. Near-infrared fluorescence sentinel lymph node mapping in breast cancer: A multicenter experience. *Breast Cancer Res. Treat*. 143(2):333–342.

Via, B. K., C. L. So, T. F. Shupe, L. G. Eckhardt, M. Stine, and L. H. Groom. 2005. Prediction of wood mechanical and chemical properties in the presence and absence of blue stain using two near infrared instruments. *J. Near Infrared Spec*. 13(4):201–212.

Via, B. K., C. Zhou, G. Acquah, W. Jiang, and L. Eckhardt. 2014. Near infrared spectroscopy calibration for wood chemistry: Which chemometric technique is best for prediction and interpretation? *Sensors-Basel* 14(8):13532–13547.

Wójciak, A., H. Kasprzyk, E. Sikorska, A. Krawczyk, M. Sikorski, and A. Wesełucha-Birczyńska. 2014. FT-Raman, FT-infrared and NIR spectroscopic characterization of oxygen-delignified kraft pulp treated with hydrogen peroxide under acidic and alkaline conditions. *Vib. Spectrosc*. 71:62–69.

Workman, J. J. and L. Weyer. 2007. Practical Guide to Interpretive Near-infrared Spectroscopy. CRC Press, Boca Raton, Florida. 344 pp.

Wu, Y., D. G. Zhou, S. Q. Wang, Y. Zhang, and C. Xing. 2009. Relationship of wood FA and density with elastic modulus. *J. Nanjing Forestry Univ*. 33(4):113–116.

Xu, J. R., W. Song, S. Y. Zou, and W. D. Zhang. 2000. Research status and some consideration in genetic improvement of elm species. *J. Beijing Forestry Univ*. 22(6):95–99.

Yan, Y. L., B. Chen, D. Z. Zhu, and L. D. Zhang. 2013. Near Infrared Spectroscopy Principle, Technology and Application. China Light Industry Press, Beijing.

Yang, Z., B. Lv, A. M. Huang, Y. N. Liu, and X. Q. Xie. 2012. Rapid identification of softwood and hardwood by near infrared spectroscopy of cross-sectional surfaces. *Spectrosc. Spect*. *Anal*. 32(7):1785–1789.

Zhang, R., Z. F. Li, and J. J. Pan. 2017. Coupling discrete wavelet packet transformation and local correlation maximization improving prediction accuracy of soil organic carbon based on hyperspectral reflectance. *Trans. Chin. Soc. Agric. Eng*. 33(1):175–180.

Zhi, J. J., J. W. Sun, Z. C. Wang, and W. J. Ding. 2018. Support vector machine classifier for prediction of the metastasis of colorectal cancer. *Int. J. Mol. Med*. 41(3):1419–1426.

Zhuang, X. G., L. L. Wang, Q. Chen, X. Y. Wu, and J. X. Fang. 2017. Identification of green tea origins by near-infrared (NIR) spectroscopy and different regression tools. *Sci. China Technol. Sci*. 60(1):84–90.

http://prime-pdf-watermark.prime-prod.pubfactory.com/ | 2024-12-26